CRYSTALLIZATION

A π-gel scaffold for assembling fullerene to photoconducting supramolecular rods

10.1126/sciadv.1600142

Vishnu Sukumaran Nair,[1,2] Rahul Dev Mukhopadhyay,[1,2] Akinori Saeki,[3] Shu Seki,[4] Ayyappanpillai Ajayaghosh[1,2]*

Nonequilibrium self-assembly of molecules holds a huge prospect as a tool for obtaining new-generation materials for future applications. Crystallization of neutral molecules within a supramolecular gel matrix is one example in which two nonequilibrium processes occur orthogonal to each other. On the other hand, electronically interacting donor-acceptor two-component systems are expected to form phase-miscible hybrid systems. Contrary to the expectation, we report the behavior of a π-gel, derived from oligo(*p*-phenylenevinylene), OPVA, as a scaffold for the phase separation and crystallization of fullerene (C_{60}) to supramolecular rods with increased transient photoconductivity ($\phi\Sigma\mu_{max} = 2.4 \times 10^{-4}$ cm^2 V^{-1} s^{-1}). The C_{60} supramolecular rods in the π-gel medium exhibited high photocurrent in comparison to C_{60} loaded in a non–π-gel medium. This finding provides an opportunity for large-scale preparation of micrometer-sized photoconducting rods of fullerenes for device application.

INTRODUCTION

Systems produced by equilibrium self-assembly represent a state of energetic minima and persist for a long time due to their thermodynamic stability. These systems are inert in working on their surroundings and require an external energy source to undergo a structural transformation (*1*, *2*). On the other hand, self-assembly of molecules under nonequilibrium conditions can lead to complex architectures with fascinatingly dynamic and adaptive properties (*3*, *4*). Both crystallization and gelation of organic molecules are known to occur under conditions that are far from equilibrium (*1*, *2*). Specifically, gelation follows a nucleation growth mechanism driven by the kinetically controlled supersaturation gradient reasonably similar to the crystallization process (*1*, *5*). The nucleation process leads to the formation of one-dimensional (1D) structures with high aspect ratio, which further assemble into a 3D network, better known as self-assembled fibrillar networks that encapsulate the solvent in which they form, resulting in gelation (*6*, *7*). Gel phase crystallization has therefore drawn incredible attention to gain essential understanding of two simultaneously occurring orthogonal self-assembly processes (*1*, *8*). Supramolecular gel fibers can even act as active nucleation substrates for the crystallization of organic molecules (*9*, *10*). Weak and flexible behavior of supramolecular assembly, especially in low–molecular weight gelators, helps easy recovery of crystals from the gel matrix. Depending on the degree of interaction between the gelator and the crystallizing unit, mesoscopic compartmentalization through self-sorting or intimately mixed nanoscale phase-segregated heteroassembly can be the two possible extreme ends in these multicomponent systems (*11*). In systems that have a weak interaction between the two principal components, these nonequilibrium processes influence or modify the outcome of the assemblies to undergo nano- to mesoscale compartmentalization without losing the distinct identity of the individual components.

If such a hybrid assembly is composed of an electron donor and acceptor, it can give rise to bulk heterojunctions at varied length (nano- to meso-) scales, which are important for efficient exciton migration toward respective electrodes in an organic optoelectronic device (*12*, *13*). Among various electron-rich π-conjugated small molecular gelators, oligo(*p*-phenylenevinylene)s (OPVs) occupy a unique position because of their excellent optoelectronic properties (*14*–*16*). Proper functionalization of OPV molecules results in splendid supramolecular nanostructures that can function as scaffolds for exciton diffusion and energy transfer (*15*). The quest for new molecules and materials has also drawn the attention of material chemists toward the interaction of electron-deficient molecules, such as fullerenes (C_{60} and C_{70}), carbon nanotubes, and graphene, with OPVs (*15*–*20*). These studies have resulted in new hybrid materials of nanoscale to mesoscale morphology having donor-acceptor heterojunctions, which play a major role in the development of a variety of organic electronic devices (*21*–*24*). In this context, fullerenes have been playing a major role as electron-accepting materials. Depending on the donor medium and experimental conditions, fullerenes tend to aggregate differently to generate nanostructures of diverse shape and dimensions (*25*–*29*). All these fullerene nanostructures retain their inherent optoelectronic properties, hence having significant fundamental applications as those of solar cells, field effect transistors, and superconducting materials (*26*, *29*–*32*). Therefore, in the search for new hybrid materials, fullerenes and π-conjugated systems remain as an attractive choice for scientists (*33*–*37*). π-Conjugated systems, particularly π-gels, have a strong tendency of interacting with C_{60} (*14*). Interaction of C_{60} and C_{60} derivatives with gels and other media is known in the literature (*22*, *38*–*44*). For example, crystallization of C_{60} in *bis*-urea–based gels forms C_{60} rods (*40*). However, the electronic properties of such hybrid gels are not explored. Similarly, the interaction of a π-system with a C_{60} derivative functionalized with an imidazole moiety was reported (*38*). Note that functionalized C_{60} is inferior with respect to electronic properties. In contrast, crystallization of pristine C_{60} has more relevance and continues to be a challenge. Therefore, preparation of hybrid materials comprising pristine C_{60} with π-systems, insights on their mode of interaction, morphological features of the resulting composites, and their electronic properties are of great interest.

[1]Photosciences and Photonics Section, Chemical Sciences and Technology Division, Council of Scientific and Industrial Research–National Institute for Interdisciplinary Science and Technology (CSIR-NIIST), Thiruvananthapuram 695019, India. [2]Academy of Scientific and Innovative Research, CSIR-NIIST Campus, Thiruvananthapuram 695019, India. [3]Department of Applied Chemistry, Graduate School of Engineering, Osaka University, 2-1 Yamadaoka, Suita, Osaka 565-0871, Japan. [4]Department of Molecular Engineering, Graduate School of Engineering, Kyoto University, Katsura, Nishikyo-ku, Kyoto 615-8510, Japan.
*Corresponding author. Email: ajayaghosh@niist.res.in

The organic gel medium has already been reported as a useful scaffold for the crystallization of polymorphic pharmaceutical molecules (*7*, *45*, *46*). Encouraged by these studies, we attempted to understand the behavior of C_{60} in an OPV-based π-gel matrix. The outcome of this study reveals parallel gelation and crystallization process of OPVs and C_{60}, respectively, leading to phase separation and crystallization of C_{60} to supramolecular rods with high photoconductivity.

RESULTS

Synthesis and characterization of hybrid gel assembly

π-Gelators have a strong affinity toward carbon allotropes, such as C_{60}, carbon nanotubes, and graphene (*44*, *47*). Gelators of extended π-systems, such as OPV gelators, are expected to interact with C_{60} in aliphatic and aromatic hydrocarbon solvents (*22*, *40*, *44*). With the objective of preparing hybrid π-gels with improved electronic properties, we studied the interaction of C_{60} in different ratios with the π-gelator OPVA in toluene (Fig. 1). It is observed that the gel melting temperature (T_{gel}), which is a direct measure of gel stability, increases with the addition of each fullerene equivalent (Fig. 2A). Enhancement in the T_{gel} values indicates that the colloidal assemblies in the hybrid gels are sufficiently stronger than the bare OPVA gelator. It was observed that the rate of increase in gel strength was much faster up to 2 eq of C_{60}, wherein the gel strength increases with a steeper slope (1.25). From 2 to 6 eq of C_{60} addition, the rate of increase in gel melting temperature is almost reduced to half (slope, 0.625) before getting saturated (Fig. 2A). To compare the mechanical strength of the OPVA and the OPVA/C_{60}

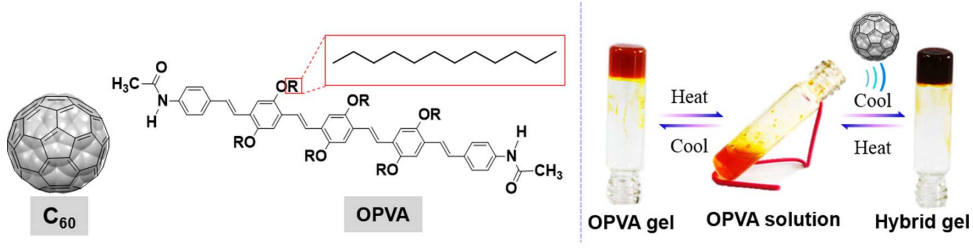

Fig. 1. Molecular structures and hybrid gel preparation. The structures of molecules used in this study and thermoreversible gelation of OPVA with and without fullerene (C_{60}).

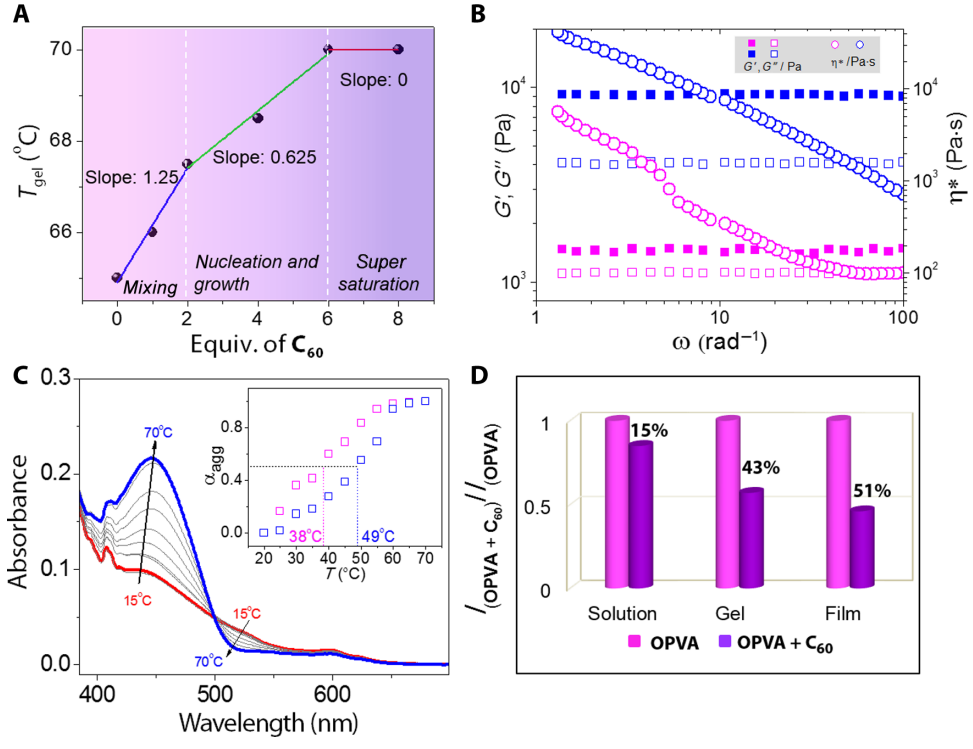

Fig. 2. Improved stability of hybrid gel and aggregates. (**A**) T_{gel} as a function of fullerene concentration. (**B**) Rheological data of OPVA (5×10^{-4} M) and OPVA/C_{60} (1:6) showing a change in the complex viscosity (η*), storage modulus (*G*′), and loss modulus (*G*″) with angular frequency (ω). (**C**) Variable temperature absorption spectra of OPVA/C_{60} (1:6) in toluene (concentration of OPVA, 1×10^{-5} M). Inset shows variation of fraction of aggregates (α_{agg}) with temperature (*T*). (**D**) Extent of emission quenching in OPVA/C_{60} hybrid in different states (all emission spectra have been obtained by exciting at 440 nm and normalized for comparison).

(1:6) hybrid gel, we performed rheological measurements. The rheological response as a function of the angular frequency at a fixed strain for OPVA gels with and without C_{60} is illustrated in Fig. 2B. Both gels showed a plateau region when the angular frequency was varied from 100 to 1 rad s^{-1}. Both gels show a substantial elastic response, and the G' values are greater than the G'' values over the entire range of frequencies. By the addition of fullerene, the value of G' was found to increase by an order of magnitude in comparison to OPVA. The ratio of G' and G'' is higher for the hybrid gel than that for the OPVA gel, indicating the better robustness of the former. The quasi-solid nature of the composite gel is higher (tan $\delta = G''/G' = 0.43$ to 0.45) than that of the OPVA gel (tan $\delta = 0.75$ to 0.77) (*48*). The complex viscosity (η^*) of the hybrid gel was also found to be higher when compared to the OPVA gel.

Variable temperature absorption studies in the solution state (1×10^{-5} M, toluene) provided evidence for the influence of C_{60} on the supramolecular assembly of OPVA (Fig. 2, C and D). Upon aggregation, absorbance at λ_{max} (440 nm) decreases with a notable blue shift for both OPVA as well as OPVA/C_{60} (1:6). Although this observation indicates the formation of H-type aggregates in both cases (*49*), there is considerable difference in the thermal stability of the aggregates (see Fig. 2C, inset, and fig. S1A). Melting transition temperature (T_m; temperature at which $\alpha_{agg} = 0.50$) for hybrid aggregates ($T_m = 49°C$) is found to be higher than that of the self-assembled aggregates of OPVA ($T_m = 38°C$). Greater thermal stability of the hybrid aggregates can be attributed to the close packing of the molecules, which is further reflected in the increased photophysical interaction of the π-gelator and C_{60} from solution to gel to film state (see Fig. 2D and fig. S1).

Concentration-dependent morphological analysis

Transmission electron microscopy (TEM) analysis of OPVA xerogel revealed micrometer-long supramolecular tapes of width varying from 50 to 100 nm (Fig. 3A). TEM images of C_{60} showed the formation of clusters ranging in size from 100 to 200 nm (Fig. 3B). This observation fairly matches with the atomic force microscopy (AFM) and scanning electron microscopy (SEM) analyses of both the samples (fig. S2). TEM analysis of the hybrid gels with different compositions of OPVA/C_{60} revealed the formation of C_{60} clusters and rods on the supramolecular tapes of OPVA at varying concentrations of C_{60}. At the low molar ratio of C_{60} (1:1 to 1:2), fullerene clusters were formed, which gradually spread out to nucleate the growth of fullerene rods (fig. S3). Upon

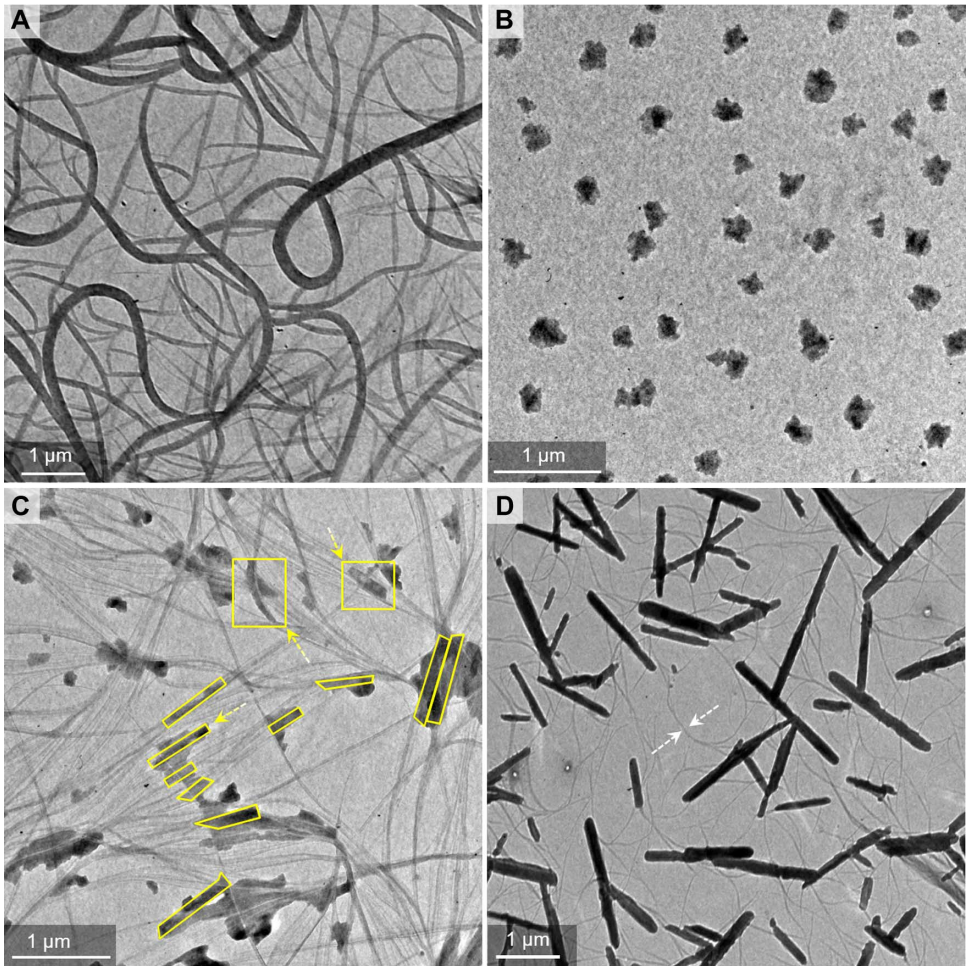

Fig. 3. TEM analysis of crystallization of C_{60} within OPVA gel matrix. (**A** to **C**) TEM image of (A) OPVA tapes, (B) C_{60} clusters, and (C) OPVA/C_{60} composite in 1:4 ratio. Fullerene domains in the OPVA matrix (yellow boxes) and yellow arrows show the growth direction of domains. (**D**) OPVA/C_{60} composite in 1:6 ratio. White arrows show supramolecular tapes of OPVA. Concentration of OPVA, 1×10^{-5} M in toluene.

increasing the concentration of fullerene (OPVA/C_{60} = 1:4), the growth of 1D fullerene domains was observed (Fig. 3C, yellow boxes). Above a 1:6 molar ratio of C_{60}, micrometer-sized crystalline fullerene rods were exclusively formed with phase-separated OPVA nanofibers (Fig. 3D, white arrows). These supramolecular rods were 1 to 2 μm in length and 125 nm in width and had a high aspect ratio (fig. S4). The restricted mobility of the solvent within the gel medium and the enhanced local concentration of C_{60} between the interstitial spaces of OPVA assemblies facilitate the nucleation of C_{60} supramolecular rods. The amide H-bond interaction and the strong π-π interactions between the OPVA molecules prevent the interaction of OPVA with C_{60}, which facilitates a phase separation between the two systems. With the gradual increase in the local supersaturation gradient of C_{60} near the supramolecular gel fibers, mesoscopic linear domains of C_{60} start to grow along the interstitial space of the bundled OPVA nanofibers. Crystallization started at this stage will be followed by an elongation process in a nonequilibrium manner to form nanorods until the local supersaturation gradient is depleted and complete mesoscale phase segregation is achieved. However, the substantial increase in the viscosity of OPVA gel with the addition of C_{60} indicates the interaction of the gelator and the solvent molecules with the C_{60} microstructures at a macroscopic level. This is clear from the TEM image in Fig. 3D, which reveals the entanglement of fullerene rods with the supramolecular tapes of OPVA (also see fig. S3C).

Fullerene nanorods grown inside the gel medium showed a molecular-level arrangement with well-ordered lattice fringes. The polycrystalline nature of the bulk fullerene (Fig. 4A) is clear from the high-resolution TEM studies and observed fast Fourier transform (FFT) pattern (Fig. 4B, inset). Careful examination of the high-resolution images and FFT patterns further proves the crystallization of fullerene rods inside the supramolecular gel medium (Fig. 4C). These fullerene rods formed in the gel medium exhibited better crystalline nature (Fig. 4D) than the fullerene crystals grown from toluene under ambient conditions. Reconstructed high-resolution TEM (HRTEM) image of the fullerene rods clearly shows crystallized C_{60} domains (Fig. 4E). The presence of C_{60} was confirmed by taking a line profile in Fig. 4E, whereby a distance of 0.79 nm was repeatedly observed between regions of same contrast (Fig. 4G). This value fairly matches the diameter (0.71 nm) of a C_{60} molecule (Fig. 4F) and the HRTEM image of C_{60} reported in literature (*50*).

Structural elucidation from x-ray diffraction experiments

Wide-angle x-ray scattering (WAXS) measurement was conducted on bulk C_{60}, OPVA xerogel, and the hybrid xerogel (Fig. 5A). The diffraction peaks obtained in bulk C_{60} matched well with the standard face-centered cubic (fcc) crystal phase [Joint Committee on Powder Diffraction Standards (JCPDS) card no. 00-043-0995] (*51*). The results also confirmed the complete absence of hexagonal close-packed (hcp) structure (fig. S5) (*52*). Diffraction peaks with *d*-spacing of 8.4, 4.4, 3.5, and 3.4 Å are indexed as (111), (311), (222), and (331) planes, respectively, from the fcc lattice. These peaks were unaltered in the hybrid xerogel, justifying a retained fcc packing of the fullerene rods, which is important for better charge transport due to close packing of the C_{60} molecules (*53*). The noticeable diffraction peaks observed in the case of OPVA xerogel includes a broad shoulder corresponding to a *d*-spacing of 32.1 Å, a sharp peak corresponding to 15.7 Å, and a

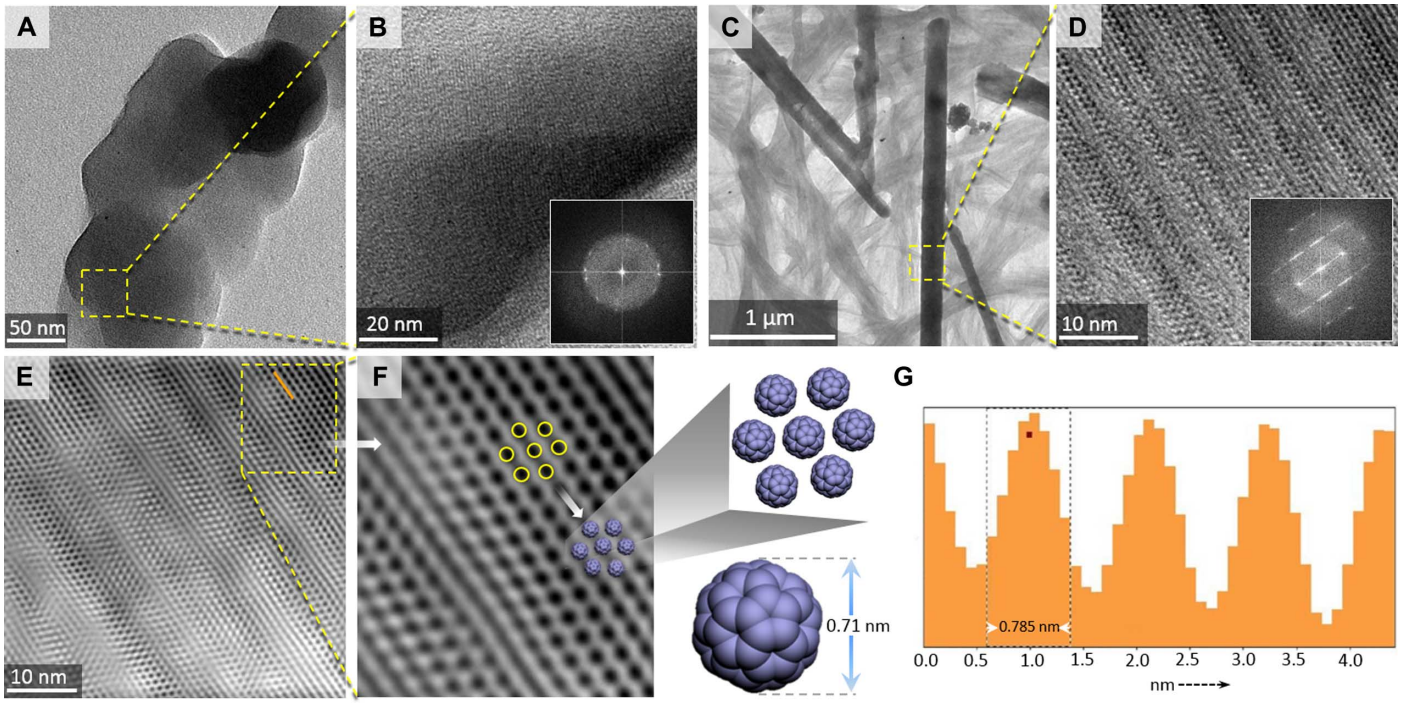

Fig. 4. HRTEM analysis of gel-assisted fullerene assembly. (**A** to **D**) HRTEM images of (A and B) bulk C_{60} and (C and D) C_{60} rods grown inside the gel medium. Insets show respective FFT patterns of the images. (**E**) Processed image of (D) using the Gatan Microscopy Suite software. (**F**) Magnified image of the area in yellow box of (E) showing closely packed fullerenes in yellow circles. Molecular dimensions of C_{60} is represented. (**G**) Line profile corresponding to the orange line drawn in image (E).

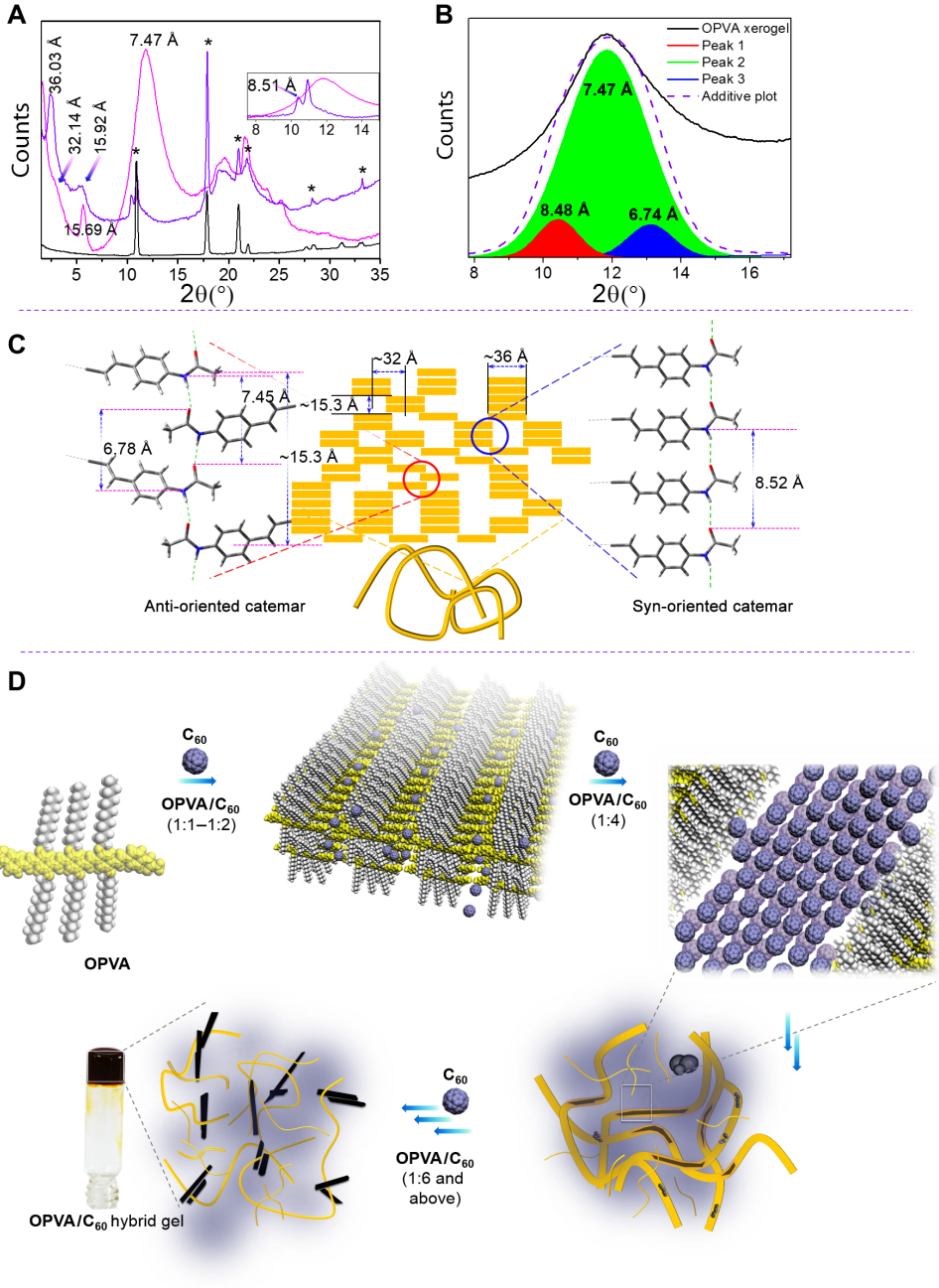

Fig. 5. WAXS analysis to elucidate the plausible mechanism of orthogonal self-assembly. (**A**) WAXS pattern of OPVA (pink), OPVA/C_{60} (1:6) (violet), and C_{60} (black). (**B**) Deconvoluted spectra of the x-ray diffraction (XRD) peak of OPVA at 7.47 Å. (**C**) Schematic representation of anti- and syn-oriented catemer formation in OPVA assembly, leading to the formation of tapes. (**D**) Plausible scheme of formation of C_{60} rods in OPVA/C_{60} composites.

broad, intense peak corresponding to an average *d*-spacing value of 7.47 Å. Deconvolution of the third peak gives us access to three diffraction peaks, which contribute to its broadness. Deconvoluted peaks 1, 2, and 3 correspond to a *d*-spacing value of 8.48, 7.47, and 6.74 Å, respectively (Fig. 5B). These peaks can be assigned to a mixture of syn- and anti-oriented catemers of OPVA and match well with the distance between the molecular stacks, that is, 32.1 and 15.3 Å along the width and length of the tape justifying the short- (broad shoulder) and the long-range (sharp peak) order, respectively (*49*). The presence of both syn- and anti-oriented catemers in OPVA tapes results in the variation of the distance between the planes, which contain the amide functionality in the alternately stacked OPVA molecules. This explains the broadening of the peak at 7.47 Å. In the hybrid gel, the first peak corresponds to a *d*-spacing of 36 Å, followed by a hump at

15.9 Å, and the third peak corresponds to a *d*-spacing of 8.51 Å. From our morphological investigations, we observed that on the addition of C_{60}, the OPVA tapes are chopped down into thinner fibers. A probable explanation for this observation may be that, in the hybrid gel, compartmentalization of C_{60} occurs within syn-oriented OPVA catemer domains, the width of which corresponds to the molecular length of OPVA (36 Å). The reduction in the number of anti-oriented catemers joining the syn-oriented catemer stacks in the hybrid gel results in the thinning of the OPVA tapes. The abundance of syn-oriented OPVA catemers in the thin hybrid gel fibers results in a uniform distance between the planes that contain the amide functionality (8.52 Å) between alternately stacked OPVA molecules. This is a probable explanation for the gradual shifting and sharpening of the peak (corresponding to a *d*-spacing of 8.51 Å) in the hybrid gel (Fig. 5, C and D). The molecular distances have been calculated on the basis of the crystal structure of acetanilide and benzanilide, which crystallize in the anti- and syn-oriented catemer, respectively (*54*–*56*).

Charge transport properties

Because the fullerene supramolecular rods are expected to be photoconducting, we conducted flash photolysis time-resolved microwave conductivity (FP-TRMC) measurement, which is an electrodeless technique for evaluating intrinsic photoconductivity of the material with minimum trapping effects (*57*, *58*). The quantification of intrinsic photoconductivity in terms of $\phi\Sigma\mu$ values is shown in Fig. 6A, where ϕ is the charge-carrier generation quantum yield upon photoexcitation and $\Sigma\mu$ represents the sum of charge-carrier mobilities. The maximum value ($\phi\Sigma\mu_{max}$) usually signifies the intrinsic short-range charge-carrier mobility. The measurements showed a $\phi\Sigma\mu_{max}$ value of 2.0×10^{-5} and 2.5×10^{-5} $cm^2\ V^{-1}\ s^{-1}$ for OPVA/C_{60} blends with a molar ratio of 1:2 and 1:4, respectively. The $\phi\Sigma\mu_{max}$ increases by ~22-fold to a value of 2.4×10^{-4} $cm^2\ V^{-1}\ s^{-1}$ (Fig. 6B) for a 1:6 blend ratio of OPVA/C_{60}, as compared to that of OPVA xerogel ($\phi\Sigma\mu_{max} = 1.1 \times 10^{-5}$ $cm^2\ V^{-1}\ s^{-1}$). The sudden increase found between OPVA/C_{60} = 1:6 and OPVA/C_{60} = 1:4 is probably due to the increase in $\Sigma\mu$ because of better electron percolation pathways in the extended fullerene nanorod (*59*).

Furthermore, the electrical transport in the fullerene rods is studied by photocurrent measurement of spin-coated xerogel samples on organic field effect transistor platform (Fig. 6C) (*53*, *60*, *61*). Current-voltage (*I*-*V*) characteristics illustrate considerable enhancement in the photocurrent with increases in C_{60} content in OPVA/C_{60} blends. Random aggregates formed at the low concentration of C_{60} do not conduct well because of nanoscale discontinuity combined with dimensional limitations, which is already demonstrated in morphological studies. As the ratio of fullerene increases, photoresponse of the composite enhances hinting toward the importance of nano- to mesoscale phase segregation and formation of heterojunctions in the transport properties. Advantages of long-range mesoscale phase segregation and molecular space confinement in the fullerene rods facilitate the efficient charge transport at 6 eq of fullerene and above.

Supramolecular gel-assisted growth of fullerene rods is an interesting example of gel phase crystallization. Gelation and crystallization are two orthogonal processes, which occur at different rates. The outcome and properties of the resultant nanostructures from these orthogonal assemblies depend on effective phase separation, which in turn depends on the weak and slow interaction between gelator and crystallizing

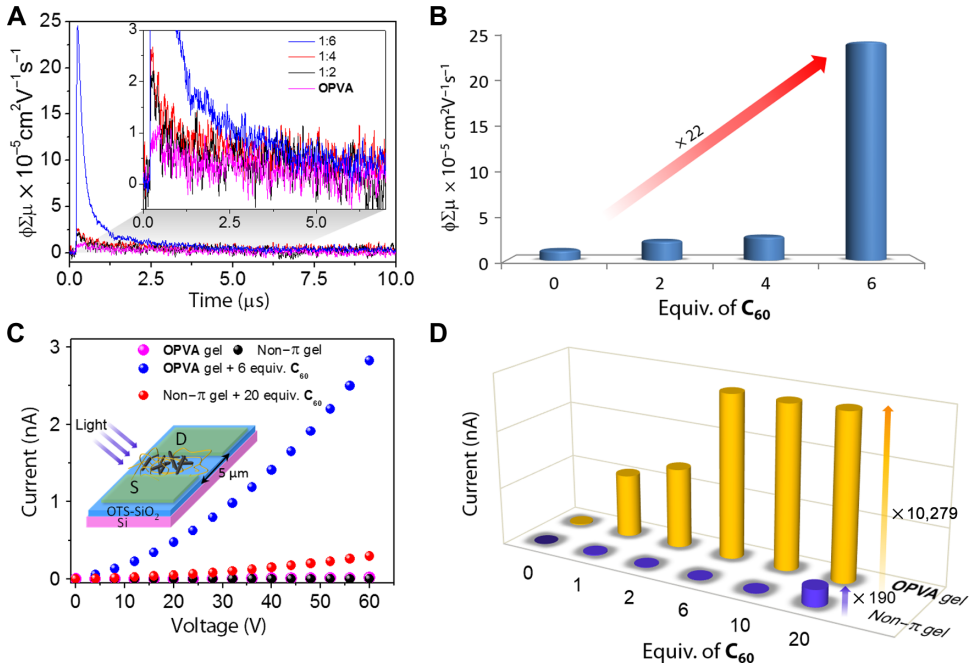

Fig. 6. Photoconductivity from the coassembled hybrid nanostructures. (**A**) FP-TRMC data for OPVA with different ratio of C_{60}. Graph is zoomed to show the variation of conductivity in the lower ratio of C_{60}. (**B**) Secondary plot showing the variation of the $\phi\Sigma\mu$ value for OPVA with different ratios of C_{60}. The value increases 22-fold in the case of OPVA/C_{60} (1:6) blend. (**C**) *I*-*V* characteristics of gelators and their respective hybrid samples (at the bias voltage of 20 V). Inset shows the device configuration. (**D**) Comparison of photocurrent generation from C_{60} in two different gel media (concentration of gelator, 1×10^{-5} M in toluene). Upon addition of 20 eq of C_{60}, the photocurrent generated is ~10^4 times in OPVA, whereas a 190-fold increase is found in the non–π-gelator (*2*).

substrate in this multicomponent assembly. Therefore, to justify the effect of the π-gel medium, OPVA was replaced by *n*-decanamide (**2**), which is a non–π-conjugated gelator (fig. S6). When compared to the OPVA/C_{60} system, the hybrid gel obtained from **2**/C_{60} showed low photoconductivity (Fig. 6, C and D), although the formation of nanoscale C_{60} rods is reported in case of gelators without a π-backbone (*40*). Reversible photoresponse of the fullerene nanostructures from both gels is illustrated in the photocurrent time profile (fig. S7). It is observed that excess loading of C_{60} is required in the gel matrix of **2** to generate a substantial photoresponse. Therefore, it can be said that more than acting as a medium for crystallization, the supramolecular gel matrix of OPVA plays the role of an active material, which connects nanorods with each other, having continuous charge carrier pathway in micrometer dimensions. In contrast to the π-gel medium, **2** provides an insulating environment that reduces electrical transportability.

DISCUSSION

The supramolecular tapes of the OPVA π-gelator are found to be excellent scaffolds for the crystallization of C_{60} as supramolecular rods. Phase separation and orthogonal self-assembly of OPVA and C_{60} occur within the gel medium, resulting in hybrid gels comprising crystalline fullerene rods. The strong π-π interaction and H-bonding between the OPVA molecules prevent OPVA-C_{60} interaction, thus facilitating the phase separation between the two. Morphological studies established the concentration dependency of the supramolecular rod formation. The supramolecular gel medium slows down the rate of crystallization of C_{60} molecules. Crystallization at a slower rate results in molecular-level ordering, which leads to higher crystallinity of the supramolecular fullerene rods. The C_{60} rods formed in the π-gel medium exhibited relatively high photocurrent generation when compared to C_{60} dispersed in a non–π-gel medium. Formation of donor-acceptor heterojunctions in nanoscale level is proved by transient photoconductivity measurements. Transient conductivity depends on the composition ratio of fullerene, which in turn also affects the nano- to mesoscale morphology of this orthogonal self-assembling system. This study opens up the possibility of exploring a variety of π-gels as scaffolds for the assembly of carbon allotropes and their use in optoelectronic applications.

MATERIALS AND METHODS

Synthesis: General procedures

Unless otherwise stated, all organic starting materials and reagents were purchased from commercial suppliers and used without further purification. Amide-functionalized oligo(*p*-phenylenevinylene)–based gelator (OPVA) was synthesized according to the reported procedure and characterized by standard methods (*49*).

Gelation studies

The compound was taken in a sealed glass vial with a known volume of solvent. The glass vial was heated until the compound dissolved. Gel formation occurred when the hot solution was allowed to cool and was confirmed by the incapability of the content to flow when inverting the glass vial. Repeated heating and cooling of the solution confirmed the thermal reversibility of the supramolecular gel. T_{gel} was determined by the dropping ball method (*49*).

Rheology experiments

The rheological properties of the OPVA and the hybrid gels with C_{60} were measured using a Physica Modular Compact (MCR 150) stress-controlled rheometer from Anton Paar with a cone-and-plate geometry (CP 50-1). A parallel plate sensor 50 mm in diameter was used to maintain a gap size of 0.1 mm. Gels in toluene were transferred to the peltier, and the plate was covered properly to avoid the solvent evaporation. Dynamic oscillatory mode was used for the measurements, keeping a constant strain amplitude (γ) of 1%, and the angular frequency was varied from 1 to 100 $rads^{-1}$.

Electronic spectral measurements

A Shimadzu UV-3101 PC NIR scanning spectrophotometer was used to record the electronic absorption spectra, and the emission spectra were recorded on a SPEX Fluorolog FL-1039 spectrofluorimeter. All optical measurements were carried out using 0.1- or 1-cm cuvettes with a thermistor directly attached to the wall of the cuvette holder for controlling the temperature.

Morphological analysis

An NTEGRA (NT-MDT) operating with a tapping mode regime was used to record AFM images under ambient conditions. Microfabricated TiN cantilever tips (NSG10) with a resonance frequency of 299 kHz and a spring constant of 20 to 80 $N\,m^{-1}$ were used. AFM section analysis was done offline. Samples for the imaging were prepared by drop-casting toluene solution of OPVA, C_{60}, and OPVA/C_{60} onto a freshly cleaved mica sheet at the required concentrations under ambient conditions and were dried under vacuum. TEM measurements were carried out using FEI (Tecnai G2 30 S-TWIN) with an accelerating voltage of 100 kV. Samples were prepared by drop-casting toluene solutions of OPVA, C_{60}, and OPVA/C_{60} onto carbon-coated copper grids at the required concentrations under ambient conditions. The samples were dried under vacuum. TEM images were obtained without staining. Inverse FFT reconstruction of the HRTEM images was done using the software program Digital Micrograph (Gatan Inc.), following a reported procedure (*62*). FFT of the experimentally obtained image was initially taken, followed by appropriate mask filtering to remove the spatial frequency of the diffractogram. Finally, the inverse FFT gave rise to a reconstructed HRTEM image. SEM images were obtained with a Zeiss EVO 18 cryo-SEM Special Edn with variable pressure detector working at 20 to 30 kV. Samples were prepared from toluene solutions of appropriate concentration by drop-casting onto a freshly cleaved mica surface.

XRD analysis

Samples for the XRD studies were prepared by transferring respective gels onto aluminum foil and dried slowly to evaporate the solvent. Finally, all the samples kept under vacuum to ensure complete removal of solvent. X-ray diffractogram of the dried films were recorded on a Xeuss SAXS/WAXS system using a Genix microsource from Xenocs operated at 50 kV and 0.6 mA. The Cu Kα radiation (λ = 1.54 Å) was collimated with a FOX 2D mirror and two pairs of scatterless slits from Xenocs. The 2D patterns were recorded on a Mar345 image plate and processed using the Fit2D software. All measurements were made in the transmission mode. The sample-to-detector distance was calibrated with silver behenate standard, and it was found to be 214.5 mm. Deconvolution of XRD data was performed using the Fityk 0.9.8 software (*63*).

FP-TRMC studies

The third harmonic generation (355 nm) of a Nd:YAG laser (5- to 8-ns pulse duration, Spectra Physics GCR-130; incident photon density to a sample was set to 9.1×10^{15} cm^{-2}) was used as an excitation source for TRMC. The transient photoconductivity ($\Delta\sigma$) was measured by TRMC using a 3-mW X-band (~9.1 GHz) microwave. The obtained transient photoconductivity ($\Delta\sigma$) was converted to the product of the quantum yield (ϕ) and the sum of charge carrier mobilities, ($\Sigma\mu = \mu_+ + \mu_-$), by $\phi\Sigma\mu = \Delta\sigma\,(eI_0F_{light})^{-1}$, where e, I_0, and F_{light} are the unit charge of a single electron, the incident photon density of excitation laser (in m^{-2}), and the correction (or filling) factor (in m^{-1}), respectively. The F_{light} was calculated by taking into consideration the geometry and optical properties of the sample, such as the size, laser cross section, and absorption of the excitation laser. The details of the system were previously reported (*58*). All experiments were carried out at room temperature. Samples were prepared by drop-casting toluene solutions of OPVA and OPVA/C_{60} on quartz plates and then drying under vacuum.

Photocurrent measurements

Devices for photocurrent measurement were fabricated on the organic field effect transistors (OFET) platform with bottom gate/bottom contact configuration. For gate electrode and gate dielectric layer, a heavily doped *n*-type Si wafer and dry oxidized SiO_2 were used, respectively (capacitance of 11 nF cm^{-2}) (*64*). Thickness of the dielectric was 300 nm, with surface roughness less than 0.1 nm. Gold electrodes were used as both source and drain. Photolithography technique has been used to deposit gold electrodes. After sequential washing with water, deionized water, and ethanol, substrates were rinsed with acetone. Surface modification of all substrates was done with *n*-trichloro(octadecyl)silane, followed by cleaning with *n*-hexane, $CHCl_3$, and acetone. The system was kept under vacuum for 60 min, and the substrates were washed with ethanol. OPVA, OPVA/C_{60}, **2**, and **2**/C_{60} were dissolved in toluene, heated, and cooled to obtain a gel in individual cases. The gels were further diluted with toluene and spin-coated, as mentioned above, with modified silicon substrate at 2000 rpm for 30 s. Samples were kept under vacuum overnight at room temperature to ensure complete removal of the solvent. Photocurrent measurement of the devices was carried under ambient conditions, using a Keithley Model 4200 SCS semiconductor parameter analyzer.

SUPPLEMENTARY MATERIALS

Supplementary material for this article is available at http://advances.sciencemag.org/cgi/content/full/2/9/e1600142/DC1

fig. S1. Photophysical studies of OPVA and OPVA/C_{60} (1:6) hybrid assembly.
fig. S2. Morphological characterization of OPVA, C_{60}, OPVA/C_{60} (1:6) hybrid.
fig. S3. Nucleation and growth of C_{60} supramolecular rods within the OPVA gel matrix.
fig. S4. Size distribution of C_{60} supramolecular rods based on TEM analysis.
fig. S5. XRD analysis of C_{60}.
fig. S6. Effect of gelator on photocurrent generation.
fig. S7. On/off switching of photocurrent.
References (*51*, *52*)

REFERENCES AND NOTES

1. D. K. Kumar, J. W. Steed, Supramolecular gel phase crystallization: Orthogonal self-assembly under non-equilibrium conditions. *Chem. Soc. Rev.* **43**, 2080–2088 (2014).
2. E. Mattia, S. Otto, Supramolecular systems chemistry. *Nat. Nanotechnol.* **10**, 111–119 (2015).
3. P. A. Korevaar, S. J. George, A. J. Markvoort, M. M. J. Smulders, P. A. J. Hilbers, A. P. H. J. Schenning, T. F. A. De Greef, E. W. Meijer, Pathway complexity in supramolecular polymerization. *Nature* **481**, 492–496 (2012).
4. T. Aida, E. W. Meijer, S. I. Stupp, Functional supramolecular polymers. *Science* **335**, 813–817 (2012).
5. J.-L. Li, X.-Y. Liu, Architecture of supramolecular soft functional materials: From understanding to micro-/nanoscale engineering. *Adv. Funct. Mater.* **20**, 3196–3216 (2010).
6. J. L. Li, X. Y. Liu, *Soft Fibrillar Materials: Fabrication and Applications* (Wiley-VCH, Weinheim, 2013), pp. 1961–2007.
7. N. Garti, I. Amar-Yuli, *Nanotechnologies for Solubilization and Delivery in Foods, Cosmetics and Pharmaceuticals* (DEStech Publications Inc., Pennsylvania, 2012), pp. 284–287.
8. R. D. Mukhopadhyay, V. K. Praveen, A. Hazra, T. K. Maji, A. Ajayaghosh, Light driven mesoscale assembly of a coordination polymeric gelator into flowers and stars with distinct properties. *Chem. Sci.* **6**, 6583–6591 (2015).
9. J. A. Foster, M.-O. M. Piepenbrock, G. O. Lloyd, N. Clarke, J. A. K. Howard, J. W. Steed, Anion-switchable supramolecular gels for controlling pharmaceutical crystal growth. *Nat. Chem.* **2**, 1037–1043 (2010).
10. O. M. Yaghi, G. Li, H. Li, Crystal growth of extended solids by nonaqueous gel diffusion. *Chem. Mater.* **9**, 1074–1076 (1997).
11. M. M. Safont-Sempere, G. Fernández, F. Würthner, Self-sorting phenomena in complex supramolecular systems. *Chem. Rev.* **111**, 5784–5814 (2011).
12. R. Charvet, Y. Yamamoto, T. Sasaki, J. Kim, K. Kato, M. Takata, A. Saeki, S. Seki, T. Aida, Segregated and alternately stacked donor/acceptor nanodomains in tubular morphology tailored with zinc porphyrin–C_{60} amphiphilic dyads: Clear geometrical effects on photoconduction. *J. Am. Chem. Soc.* **134**, 2524–2527 (2012).
13. I. D. Tevis, W.-W. Tsai, L. C. Palmer, T. Aytun, S. I. Stupp, Grooved nanowires from self-assembling hairpin molecules for solar cells. *ACS Nano* **6**, 2032–2040 (2012).
14. S. S. Babu, V. K. Praveen, A. Ajayaghosh, Functional π-gelators and their applications. *Chem. Rev.* **114**, 1973–2129 (2014).
15. V. K. Praveen, C. Ranjith, E. Bandini, A. Ajayaghosh, N. Armaroli, Oligo(phenylenevinylene) hybrids and self-assemblies: Versatile materials for excitation energy transfer. *Chem. Soc. Rev.* **43**, 4222–4242 (2014).
16. S. Yagai, S. Okamura, Y. Nakano, M. Yamauchi, K. Kishikawa, T. Karatsu, A. Kitamura, A. Ueno, D. Kuzuhara, H. Yamada, T. Seki, H. Ito, Design amphiphilic dipolar π-systems for stimuli-responsive luminescent materials using metastable states. *Nat. Commun.* **5**, 4013 (2014).
17. Z. Li, Z. Liu, H. Sun, C. Gao, Superstructured assembly of nanocarbons: Fullerenes, nanotubes, and graphene. *Chem. Rev.* **115**, 7046–7117 (2015).
18. G. Accorsi, N. Armaroli, Taking advantage of the electronic excited states of [60]-fullerenes. *J. Phys. Chem. C* **114**, 1385–1403 (2010).
19. D. M. Guldi, B. M. Illescas, C. M. Atienza, M. Wielopolski, N. Martín, Fullerene for organic electronics. *Chem. Soc. Rev.* **38**, 1587–1597 (2009).
20. P. Bairi, K. Minami, W. Nakanishi, J. P. Hill, K. Ariga, L. K. Shrestha, Hierarchically structured fullerene C_{70} cube for sensing volatile aromatic solvent vapors. *ACS Nano* **10**, 6631–6637 (2016).
21. R. Charvet, S. Acharya, J.P. Hill, M. Akada, M. Liao, S. Seki, Y. Honsho, A. Saeki, K. Ariga, Block-copolymer-nanowires with nanosized domain segregation and high charge mobilities as stacked p/n heterojunction arrays for repeatable photocurrent switching. *J. Am. Chem. Soc.* **131**, 18030–18031 (2009).
22. A. Insuasty, C. Atienza, J. L. López, J. Marco-Martínez, S. Casado, A. Saha, D. M. Guldi, N. Martín, Supramolecular one-dimensional n/p-nanofibers. *Sci. Rep.* **5**, 14154 (2015).
23. W.-S. Li, Y. Yamamoto, T. Fukushima, A. Saeki, S. Seki, S. Tagawa, H. Masunaga, S. Sasaki, M. Takata, T. Aida, Amphiphilic molecular design as a rational strategy for tailoring bicontinuous electron donor and acceptor arrays: Photoconductive liquid crystalline oligothiophene-C_{60} dyads. *J. Am. Chem. Soc.* **130**, 8886–8887 (2008).
24. J. López-Andarias, J. L. López, C. Atienza, F. G. Brunetti, C. Romero-Nieto, D. M. Guldi, N. Martín, Controlling the crystalline three-dimensional order in bulk materials by single-wall carbon nanotubes. *Nat. Commun.* **5**, 3763 (2014).
25. M. Sathish, K. Miyazawa, J. P. Hill, K. Ariga, Solvent engineering for shape-shifter *pure* fullerene (C_{60}). *J. Am. Chem. Soc.* **131**, 6372–6373 (2009).
26. S. S. Babu, H. Möhwald, T. Nakanishi, Recent progress in morphology control of supramolecular fullerene assemblies and its applications. *Chem. Soc. Rev.* **39**, 4021–4035 (2010).
27. T. Michinobu, T. Nakanishi, J. P. Hill, M. Funahashi, K. Ariga, Room temperature liquid fullerenes: An uncommon morphology of C_{60} derivatives. *J. Am. Chem. Soc.* **128**, 10384–10385 (2006).
28. L. K. Shrestha, Q. Ji, T. Mori, K. Miyazawa, Y. Yamauchi, J. P. Hill, K. Ariga, Fullerene nanoarchitectonics: From zero to higher dimensions. *Chem. Asian J.* **8**, 1662–1679 (2013).
29. D. Bonifazi, O. Enger, F. Diederich, Supramolecular [60]fullerene chemistry on surfaces. *Chem. Soc. Rev.* **36**, 390–414 (2007).
30. M. A. Lebedeva, T. W. Chamberlain, A. N. Khlobystov, Harnessing the synergistic and complementary properties of fullerene and transition-metal compounds for nanomaterial applications. *Chem. Rev.* **115**, 11301–11351 (2015).

31. Y. Iwasa, Superconductivity: Revelations of the fullerenes. *Nature* **466**, 191–192 (2010).
32. J. C. Barnes, E. J. Dale, A. Prokofjevs, A. Narayanan, I. C. Gibbs-Hall, M. Juríček, C. L. Stern, A. A. Sarjeant, Y.Y. Botros, S. I. Stupp, J. F. Stoddart, Semiconducting single crystals comprising segregated arrays of complexes of C_{60}. *J. Am. Chem. Soc.* **137**, 2392–2399 (2015).
33. Y. Yamamoto, G. Zhang, W. Jin, T. Fukushima, N. Ishii, A. Saeki, S. Seki, S. Tagawa, T. Minari, K. Tsukagoshi, T. Aida, Ambipolar-transporting coaxial nanotubes with a tailored molecular graphene–fullerene heterojunction. *Proc. Natl. Acad. Sci. U.S.A.* **106**, 21051–21056 (2009).
34. M. H. Nurmawati, P. K. Ajikumar, R. Renu, C. H. Sow, S. Valiyaveettil, Amphiphilic poly(*p*-phenylene)-driven multiscale assembly of fullerenes to nanowhiskers. *ACS Nano* **2**, 1429–1436 (2008).
35. M. J. Hollamby, M. Karny, P. H. H. Bomans, N. A. J. M. Sommerdjik, A. Saeki, S. Seki, H. Minamikawa, I. Grillo, B. R. Pauw, P. Brown, J. Eastoe, H. Möhwald, T. Nakanishi, Directed assembly of optoelectronically active alkyl–π-conjugated molecules by adding *n*-alkanes or π-conjugated species. *Nat. Chem.* **6**, 690–696 (2014).
36. V. S. Nair, Y. Pareek, V. Karunakaran, M. Ravikanth, A. Ajayaghosh, Cyclotriphosphazene appended porphyrins and fulleropyrrolidine complexes as supramolecular multiple photosynthetic reaction centers: Steady and excited states photophysical investigation. *Phys. Chem. Chem. Phys.* **16**, 10149–10156 (2014).
37. J. L. Segura, N. Martín, D. M. Guldi, Materials for organic solar cells: The C_{60}/π-conjugated oligomer approach. *Chem. Soc. Rev.* **34**, 31–47 (2005).
38. P. Xue, P. Wang, B. Yao, J. Sun, P. Gong, Z. Zhang, C. Qian, R. Lu, Nanofibers of hydrogen-bonded two-component gel with closely connected p- and n-channels and photoinduced electron transfer. *ACS Appl. Mater. Interfaces* **6**, 21426–21434 (2014).
39. P. Xue, P. Wang, B. Yao, J. Sun, P. Gong, Z. Zhang, R. Lu, Photocurrent generation of nanofibers constructed using a complex of a gelator and a fullerene derivative. *RSC Adv.* **5**, 75425–75433 (2015).
40. C. Zhang, J. Wang, J.-J. Wang, M. Li, X.-L. Yang, H.-B. Xu, Supramolecular gel-assisted formation of fullerene nanorods. *Chemistry* **18**, 14954–14956 (2012).
41. T. Hasobe, A. S. D. Sandanayaka, T. Wada, Y. Araki, Fullerene-encapsulated porphyrin hexagonal nanorods. An anisotropic donor–acceptor composite for efficient photoinduced electron transfer and light energy conversion. *Chem. Commun.* 3372–3374 (2008).
42. P. Xue, R. Lu, L. Zhao, D. Xu, X. Zhang, K. Li, Z. Song, X. Yang, M. Takafuji, H. Ihara, Hybrid self-assembly of a π gelator and fullerene derivative with photoinduced electron transfer for photocurrent generation. *Langmuir* **26**, 6669–6675 (2010).
43. X. Yang, G. Zhang, D. Zhang, D. Zhu, A new ex-TTF-based organogelator: Formation of organogels and tuning with fullerene. *Langmuir* **26**, 11720–11725 (2010).
44. S. K. Samanta, K. S. Subrahmanyam, S. Bhattacharya, C. N. R. Rao, Composites of graphene and other nanocarbons with organogelators assembled through supramolecular interactions. *Chemistry* **18**, 2890–2901 (2012).
45. C. Daiguebonne, A. Deluzet, M. Camara, K. Boubekeur, N. Audebrand, Y. Gérault, C. Baux, O. Guillou, Lanthanide-based molecular materials: Gel medium induced polymorphism. *Cryst. Growth Des.* **3**, 1015–1020 (2003).
46. J. Buendía, E. Matesanz, D. K. Smith, L. Sánchez, Multi-component supramolecular gels for the controlled crystallization of drugs: Synergistic and antagonistic effects. *CrystEngComm* **17**, 8146–8152 (2015).
47. S. Srinivasan, S. S. Babu,V. K. Praveen, A. Ajayaghosh, Carbon nanotube triggered self-assembly of oligo(*p*-phenylene vinylene)s to stable hybrid π-gels. *Angew. Chem. Int. Ed.* **47**, 5746–5749 (2008).
48. M.-O. M. Piepenbrock, G. O. Lloyd, N. Clarke, J. W. Steed, Metal- and anion-binding supramolecular gels. *Chem. Rev.* **110**, 1960–2004 (2010).
49. S. S. Babu, V. K. Praveen, K. K. Kartha, S. Mahesh, A. Ajayaghosh, Effect of the bulkiness of the end functional amide groups on the optical, gelation, and morphological properties of oligo(*p*-phenylenevinylene) π-gelators. *Chem. Asian J.* **9**, 1830–1840 (2014).
50. A. Goel, J. B. Howard, J. B. V. Sande, Size analysis of single fullerene molecules by electron microscopy. *Carbon* **42**, 1907–1915 (2004).
51. P. W. Stephens, L. Mihaly, P. L. Lee, R. L. Whetten, S.-M. Huang, R. Kaner, F. Deiderich, K. Holczer, Structure of single-phase superconducting K_3C_{60}. *Nature* **351**, 632–634 (1991).
52. W. Krätschmer, L. D. Lamb, K. Fostiropoulos, D. R. Huffman, Solid C_{60}: A new form of carbon. *Nature* **347**, 354–358 (1990).
53. H.-X. Ji, J.-S. Hu, L.-J. Wan, Q.-X. Tang, W.-P. Hu, Controllable crystalline structure of fullerene nanorods and transport properties of an individual nanorod. *J. Mater. Chem.* **18**, 328–332 (2008).
54. S. S. Kuduva, D. Bläser, R. Boese, G. R. Desiraju, Crystal engineering of primary cubanecarboxamides. Repetitive formation of an unexpected N-H···O hydrogen-bonded network. *J. Org. Chem.* **66**, 1621–1626 (2001).
55. D. Chopra, T. N. G. Row, Evaluation of the interchangeability of C–H and C–F groups: Insights from crystal packing in a series of isomeric fluorinated benzanilides. *CrystEngComm* **10**, 54–67 (2008).
56. H. J. Wasserman, R. R. Ryan, S. P. Layne, Structure of acetanilide (C_8H_9NO) at 113 K. *Acta Cryst.* **C41**, 783–785 (1985).
57. A. Saeki, Y. Koizumi, T. Aida, S. Seki, Comprehensive approach to intrinsic charge carrier mobility in conjugated organic molecules, macromolecules, and supramolecular architectures. *Acc. Chem. Res.* **45**, 1193–1202 (2012).
58. S. Seki, A. Saeki, T. Sakurai, D. Sakamaki, Charge carrier mobility in organic molecular materials probed by electromagnetic waves. *Phys. Chem. Chem. Phys.* **16**, 11093–11113 (2014).
59. S. Prasanthkumar, S. Ghosh, V. C. Nair, A. Saeki, S. Seki, A. Ajayaghosh, Organic donor–acceptor assemblies form coaxial p–n heterojunctions with high photoconductivity. *Angew. Chem. Int. Ed.* **54**, 946–950 (2015).
60. Y. Zhang, W. Liu, L. Jiang, L. Fan, C. Wang, W. Hu, H. Zhong, Y. Li, S. Yang, Template-free solution growth of highly regular, crystal orientation-ordered C_{60} nanorod bundles. *J. Mater. Chem.* **20**, 953–956 (2010).
61. E. R. Meshot, K. D. Patel, S. Tawfick, K. A. Juggernauth, M. Bedewy, E. A. Verploegen, M. F. L. De Volder, A. J. Hart, Photoconductive hybrid films via directional self-assembly of C_{60} on aligned carbon nanotubes. *Adv. Funct. Mater.* **22**, 577–584 (2012).
62. Y. M. Kim, J. M. Jeong, J. G. Kim, Y. J. Kim, Image processing of atomic resolution transmission electron microscope images. *J. Korean Phys. Soc.* **48**, 250–255 (2006).
63. M. Wojdyr, Fityk: A general-purpose peak fitting program. *J. Appl. Cryst.* **43**, 1126–1128 (2010).
64. Z. Cai, H. Luo, P. Qi, J. Wang, G. Zhang, Z. Liu, D. Zhang, Alternating conjugated electron donor–acceptor polymers entailing pechmann dye framework as the electron acceptor moieties for high performance organic semiconductors with tunable characteristics. *Macromolecules* **47**, 2899–2906 (2014).

Acknowledgments: We acknowledge K. K. Kartha [Council of Scientific and Industrial Research–National Institute for Interdisciplinary Science and Technology (CSIR-NIIST)] for help in the synthesis during the initial stages of this research; S. Prasanthkumar and V. C. Nair (CSIR-NIIST) for help in carrying out FP-TRMC studies; D. Zhang, G. Zhang, and Z. Liu (Key Laboratory of Organic Solids, Institute of Chemistry the Chinese Academy of Sciences, China) for general help during the photocurrent measurement; J. D. Sudha and K. Mohan of CSIR-NIIST for the rheological and TEM measurements, respectively. **Funding:** A.A. is grateful to the Department of Science and Technology (DST-SERB), Government of India, for a J. C. Bose Fellowship (SERB order no. SB/S2/JCB-11/2014, dated 9 June 2015). V.S.N. and R.D.M. are thankful to the CSIR, Government of India, for research fellowships. **Author contributions:** V.S.N. undertook the synthesis of molecules, and V.S.N. and R.D.M. performed studies. A.S and S.S. supervised the FP-TRMC studies. A.A., V.S.N., and R.D.M. analyzed the data, discussed the results, and wrote and commented on the manuscript. All authors discussed the results and commented on the manuscript. A.A. was responsible for the overall project concept, direction, and coordination. **Competing interests:** The authors declare that they have no competing interests. **Data and materials availability:** All data needed to evaluate the conclusions in the paper are present in the paper and/or the Supplementary Materials. Additional data related to this paper may be requested from A.A.

Submitted 25 January 2016
Accepted 17 August 2016
Published 23 September 2016
10.1126/sciadv.1600142

Citation: V. S. Nair, R. D. Mukhopadhyay, A. Saeki, S. Seki, A. Ajayaghosh, A π-gel scaffold for assembling fullerene to photoconducting supramolecular rods. *Sci. Adv.* **2**, e1600142 (2016).

ScienceAdvances

A #-gel scaffold for assembling fullerene to photoconducting supramolecular rods

Vishnu Sukumaran NairRahul Dev MukhopadhyayAkinori SaekiShu SekiAyyappanpillai Ajayaghosh

Sci. Adv., 2 (9), e1600142. • DOI: 10.1126/sciadv.1600142